Journal of Engineering Science and Technology
Vol. 13, No. 7 (2018) 1891 - 1904

PERFORMANCE ENHANCEMENT OF A DARRIUS 3-BLADED WIND TURBINE USING CONVERGENT-DIVERGENT DUCTING SYSTEM

ABDULLATEEF A. JADALLAH*, SAHAR R. FARAG, JINAN D. HAMDI

Department of Electromechanical Engineering, University of Technology, Iraq
*Corresponding Author: abdullateef.aljad@gmail.com

Abstract

Several studies on energy augmentation systems were achieved to improve the productivity of the wind turbines. The ducting system is one of the most important applications used for this purpose. The convergent -divergent vertical ducting system was used to enhance the performance of the turbine. The ducted wind turbine was analysed and simulated using MATLAB code built for this purpose and numerically employing ANSYS FLUENT 17.2. The performance and the airflow behaviour through the duct were presented and compared with those of the vertical axis wind turbine (VAWT). The results of both approaches were presented and compared with the experimental results for the two cases considered in this work. They showed good agreement. The power coefficient enhanced by 39.024% at the opening angle of the 20 ° and exit angle 12° angle and, the power coefficient enhanced by 35.89% at opening angle by 12° and exit angle equal to 20°. Ducting system was experienced and possessed good augmentation tool of the wind turbine performance. Experimentation and analysis of this work can easily be reflected to other configurations of wind turbine rotors

Keywords: CDVAWT, Coefficient of performance, VAWT; Turbine blades, TSR.

1. Introduction

Development of renewable energy technologies has become very important because of the global warming, high consumption of energy, and the fossil fuel waste, which highly affect the environment. This pushes to deal with alternative fuels in obtaining energy.

Wind energy has become one of the fastest growing sources of energy in recent years [1]. Vertical axis wind turbines VAWTs have favourable features such as omnidirectionality, easy to fabricate, and a heavy generator is placed on the ground, which lead to stability. Many earlier studies have examined various aspects of VAWTs, such as developments of airfoils [2], numerical simulations of flows around the turbines [3, 4], flow visualizations [5], and the applications of surrounding structures [6]. Wind power plants are mostly built on open ground for airflow. The open-air stream contains more energy than kinetic energy, and this energy was used by wind turbines to generate mechanical energy [7]. However, the spread of wind technology is still limited by the low wind speed that characterizes many regions of the world. Therefore, many research groups have tried to find new ways to speed up the effectiveness of wind speed on a rotary plane [1, 8, 9].

Effect of ducting on the horizontal axis wind turbine studied by Chaudhari et al. [7]. Jadallah et al. [10] studied the performance and productivity of the vertical axis wind turbine using different rotor geometry for both the Savonius and Darrius wind turbine. Most of these challenges and capital performance can be reduced or eliminated in traditional wind turbine systems by connecting wind turbines to a suitable duct [11]. Abu-El-Yazied et al. [12] studied duct formation and optimization of Darrius vertical axis wind turbines to maximize the produced power output utilizing the effect of ducting on the 3-bladed wind rotor was simulated with CFD solver. Wang and others studied the effect of the convergent-divergent duct on the energy production of small wind turbines, and the results showed that the increase in power output 2.2 times from the same area that swept [13]. Robert investigated the case of wind turbines covered in a section of buildings. The idea of this configuration is to harness the pressure differentials of airflow between the front and the roof of the building in order to increase the speed. Using wind duct testing and computational fluid dynamic (CFD), the wind speed shown through the shroud can increase the factor by about 1.5 [14].

This paper focuses on the concentration of wind intensity on the VAWT blade, which increases the speed of wind and thus kinetic energy. The Venturi effect represents a jet effect; in which the velocity of the fluid increases as the cross-sectional area decreases, with a decrease in the static pressure correspondingly. The velocity must increase as it passes through a constriction to satisfy the principle of continuity, while its pressure decreases to satisfy the principle of conservation of kinetic energy.

2. Design and Analysis of the Ducting System

The purpose of the convergent-divergent ducting system is to improve the wind turbines power generating capability by increasing the wind velocity inside the convergent duct and allows imparting more air mass flow rate due to contraction of the divergent part of the ducting system. Flow through the duct is assumed ideal, that is mean frictionless, and as having no rotation velocity component in the wake

region. It is also considered that the flow is incompressible and steady. Figure 1 shows the convergent-divergent duct. This configuration was proposed to attain the benefits of both convergent and divergent duct.

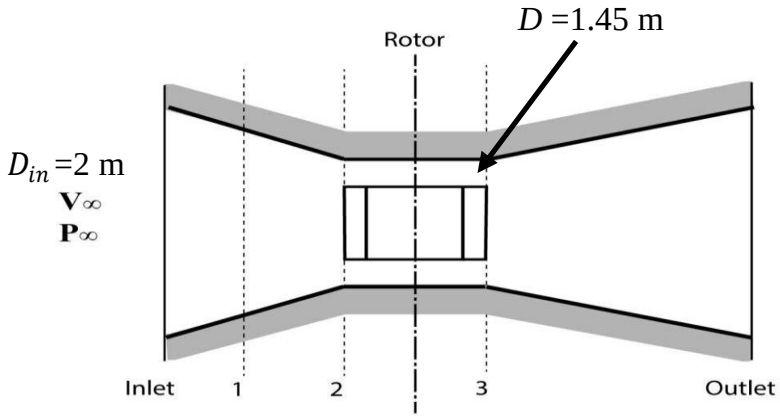

Fig. 1. Wind rotor and station numbering of the convergent-divergent duct.

This domain is divided into a series of a segment of length each of length Δx thus:

$$\Delta x = \frac{L}{N-1} \tag{1}$$

where N is the number of grid points and L is the length of the solution domain. Area at each section may be calculated as:

$$A = A_{in} - 2(A_{in} - A_n)\frac{x}{L} + (A_{in} - A_n)\frac{x^2}{L^2} \tag{2}$$

The density is constant because the flow is incompressible, so the velocity between point inlet and (2) can be calculated as [15].

$$V_i = \frac{V_{in}A_{in}}{A_i} \tag{3}$$

The velocity of the rotor initially can be calculated where ε it represents the ratio of the exit area to the entry area A_{out}/A_3, thus:

$$V_{rotor} = \varepsilon V_2(1 - a) \tag{4}$$

The pressure is then calculated for all the points.

$$P_i = P_\infty - \frac{1}{2}\rho(V_\infty^2 - V_i^2) \tag{5}$$

The convergent-divergent duct analysed by stating the area ratios of its part [16].

$$\varepsilon_c = \frac{A_2}{A_{in}} \tag{6}$$

$$\varepsilon_d = \frac{A_3}{A_{out}} \tag{7}$$

Applying Bernoulli's equation in accordance to the station numbering shown in Fig. 1 yields to when μ_{pf} is the pressure coefficient.

$$\mu_{pf} = \left[1 - \varepsilon_c^2 \frac{V_2^2}{V_\infty^2}\right] \tag{8}$$

So, doing at the exit section, the coefficient of pressure on this sector is

$$\mu_{pb} = \left[1 - \varepsilon_d^2 \frac{V_3^2}{V_\infty^2}\right] \tag{9}$$

The convergent-divergent may be analysed using Bernoulli's equation between the entrance of the convergent and wind rotor:

$$\eta_c = \frac{p_{in} - P_2}{\frac{1}{2}\rho(V_2^2 - V_{in}^2)} \tag{10}$$

Similarly, the diffuser efficiency can be defined [11]:

$$\eta_d = \frac{p_{out} - P_3}{\frac{1}{2}\rho(V_3^2 - V_{out}^2)} \tag{11}$$

The power coefficient then can be calculated from

$$Cpu = \int_{-0.5\pi}^{0.5\pi} \frac{B\omega}{4\pi V_o^3} c V_R^2 \left(C_l \sin(\alpha) - C_d \cos(\alpha)\right) d(\theta) \tag{12}$$

Similarly, the coefficient of performance in the downstream is calculated from Eq. (12) integrated for the zone of the second half of the circular trajectory of the blades.

3. Numerical Analysis of the Convergent-Divergent Ducted Wind Turbine

The process of generating the 2D CFD model was done by utilizing the ANSYS Workbench multi-physics platform where it is possible to develop a workflow. ANSYS Fluent is utilized for simulating and prediction of fluid flow properties.

3.1. Geometry

A 2D analysis for NACA0012, three airfoils are separated by 120° has been treated by ANSYS design, and then create convergent-divergent duct system for two open and exit angle 20° and 12°. Figure 2 depicts the 3D geometries of convergent-divergent duct. Figures 3 shows the two cases of convergent -divergent duct.

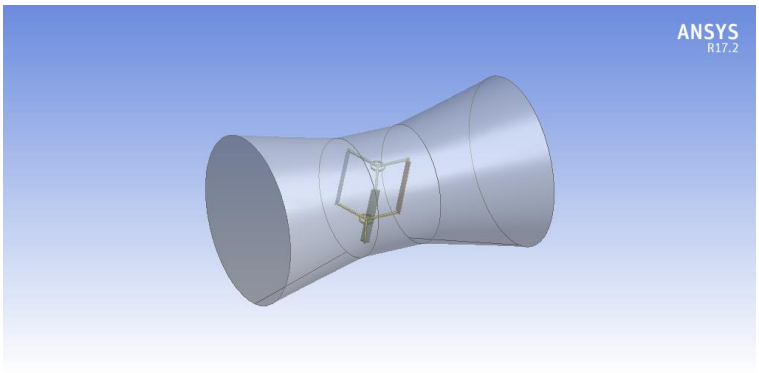

Fig. 2. 3D Geometries of ducting vertical axis wind turbine.

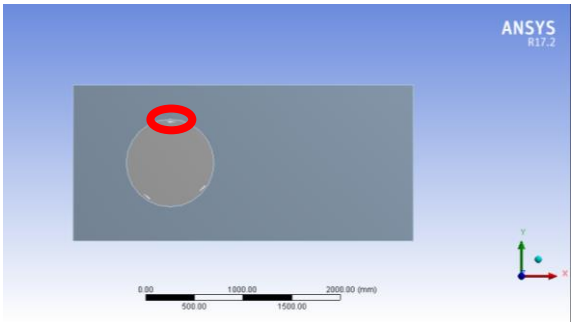

(a) Vertical axis wind turbine.

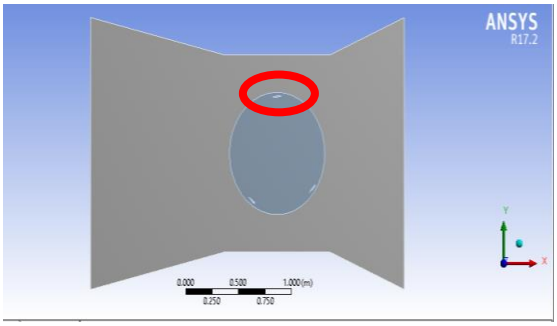

(b) Convergent-divergent duct wind turbine for open angle 12°and exit 20°.

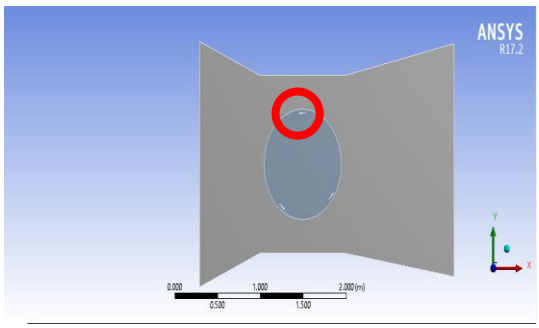

(c) Convergent-divergent duct wind turbine for open angle 20°and exit 12°.

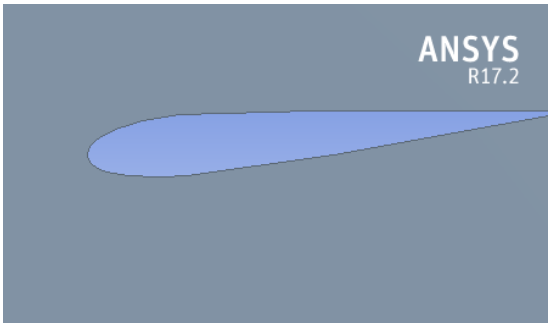

(d) Blade.

Fig. 3. 2D geometries of duct vertical axis wind turbine.

3.2. Generation of mesh:

The accuracy of results is highly depending on the mesh size and distribution. The reduction in the mesh size needs more computer memory and processing time. In the present 2-D simulations, the mesh is very fine around the blades as shown in Figs. 4. Table 1 shows all meshing characteristics.

Table 1. Meshing characteristics.

Nodes	67582
Elements	66704
Mesh Metric	Skewness
Min	2.4379e-005
Max	0.67156
Average	6.1832e-002
Standard Deviation	6.7663e-002

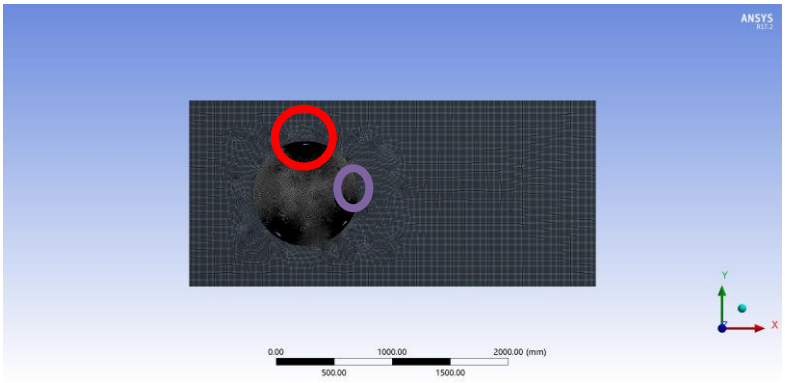

(a) Vertical axis wind turbine.

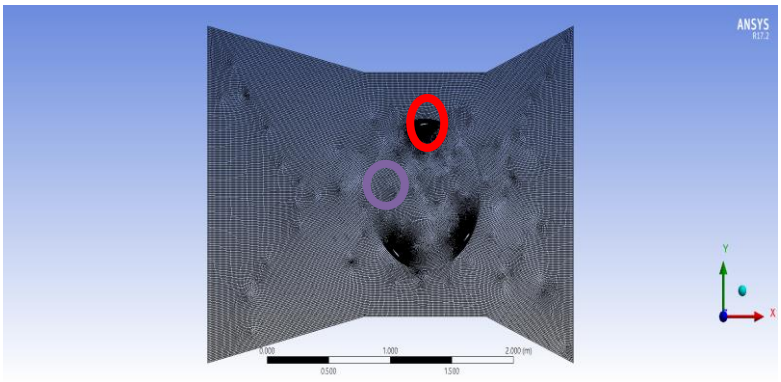

(b) Convergent-divergent duct wind turbine for open angle 12°and exit 20°.

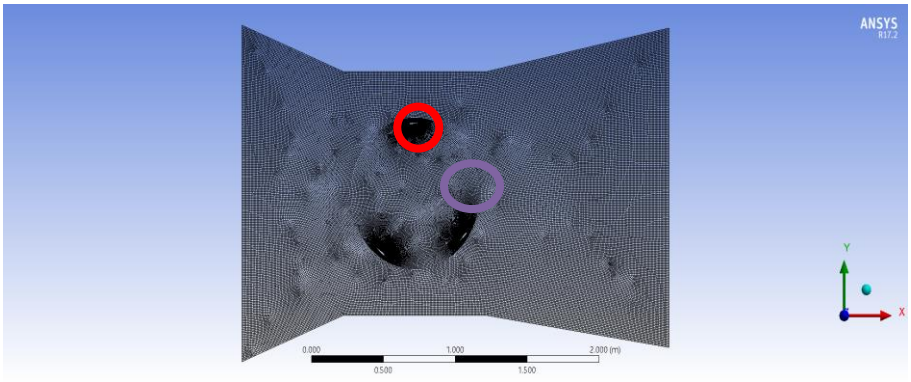

(c) Convergent-divergent duct wind turbine for open angle 20°and exit 12°.

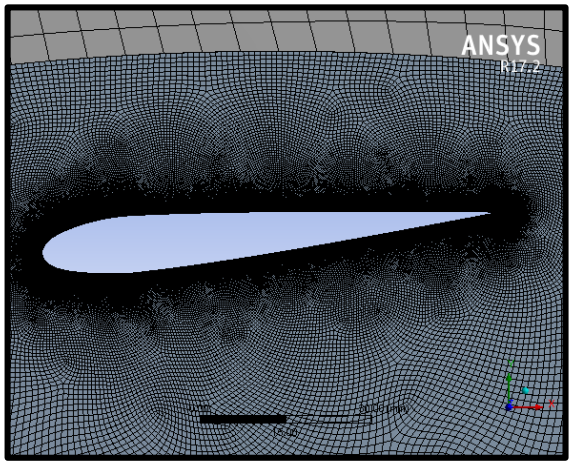

(d) Blade.

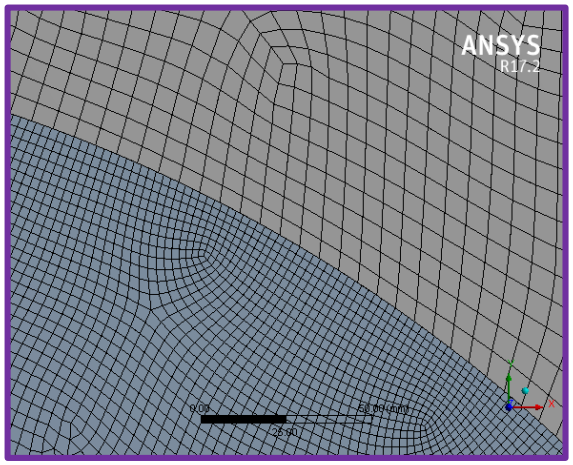

(e) Interface.

Fig. 4. 2D Meshing of ducting vertical axis wind turbine.

3.3. Boundary conditions:

Numerical investigation of the 2-D aerodynamic performance of the ducted Darrius vertical axis wind turbine is carried out using ANSYS-FLUENT 17.2. Parameters of the flow at each boundary of the flow domain are defined. The result is highly affected by the boundary conditions. There are many boundaries such as pressure at entry, inlet velocity, mass rate of flow, exit pressure etc. In this study, the boundary conditions were applied along the trajectory of the blade in order to set the rotation and location of the airfoil. In this study, wind inlet velocity has been set as inlet and pressure outlet with the value of atmospheric pressure is considered as an outlet. The domain is characterized by the ducting system. Outflow boundary condition is suitable for simulation. The magnitude of the velocity and its direction must be known. Boundary conduction in this study can be summarized in Table 2.

Table 2. Boundary conditions.

Viscous Model	
Model	K-omega
K-omega model	SST
Model constants	Default
Inlet boundary condition	
Type	Inlet velocity
Velocity specification method	Magnitude, normal to boundary
Reference Frame	Absolute
Turbulent method specification	Ratio of intensity and viscosity
Turbulent intensity %	5.0
Turbulent viscosity ratio	10.0
Outlet boundary condition	
Type	Pressure outlet
Gage pressure (Pa)	101325
Back flow direction specification method	Normal to Boundary
Turbulent specification method	Magnitude, normal to boundary
Back flow turbulence intensity %	5
Back flow, turbulent viscosity ratio	10
Computational condition	
Density (kg/m^3)	1.225
Viscosity (kg/m. s)	1.7894×10^5
Pressure (Pa)	101325

3.4. Turbulence:

The final results of the flow depend on the Reynolds number. Considering the high Reynold number needs more precision and accuracy. CFD provides a series of flow models, which may be used as per the requirement of the final results. Models and simulation approaches such as Direct Numerical Simulation (DNS), Large Eddy Simulation (LES), Detached Eddy Simulation model (DES), Reynolds Stress Model (RSM), *k*-ϵ model, *k*-ω model, Spalart-Allmaras model is available and each one of them might be effectively employed in actual applications. In the present study, wall bounded turbulent flows around the ducted Darrius wind turbine was

modelled by SST *k*-ω model. SST model for *k*-ω differs from standard model in a manner that SST ensures a change in a gradual way from standard *k*-ω model in the beneath layer having high Reynolds number flow with *k*-ϵ model in the outer region. In order to achieve this, the *k*-ϵ model is transformed into a *k*-ω formulation. Two equations eddy viscosity turbulence models are [17]:

$$\frac{\partial(\rho k)}{\partial t}+\frac{\partial(\rho u_j k)}{\partial x_j} = \mathrm{P} - \beta * \rho\omega K + \frac{\partial\left[(\mu+\sigma_k\mu_t)\frac{\partial k}{\partial x_j}\right]}{\partial x_j} \quad (13)$$

$$\frac{\partial(\rho k)}{\partial t}+\frac{\partial(\rho u_j k)}{\partial x_j} = \frac{\gamma}{v_t}\mathrm{P} - \beta * \rho\omega^2 \frac{\partial\left[(\mu+\sigma_\omega\mu_t)\frac{\partial k}{\partial x_j}\right]}{\partial x_j} + 2(1 - F_1)\frac{\rho\sigma_\omega}{\omega}\frac{\partial(k)}{\partial x_j} \ldots\ldots \quad (14)$$

4. Results and Discussion

CFD techniques are utilized to study the behavior of the airflow through venture (convergent-divergent) duct with and without turbine. Conditions are considered as per International Standard Atmosphere (ISA) and normal temperature and pressure (NTP) conditions. Inlet velocity was taken as 10 m/s in *x*-direction. CFD analysis was carried out on a venture with turbines. Figures 5 and 6 show pressure difference between the upper and lower surface of airfoil leading to an aerodynamic lift force. This aerodynamic lift causes rotation of the turbine blades.

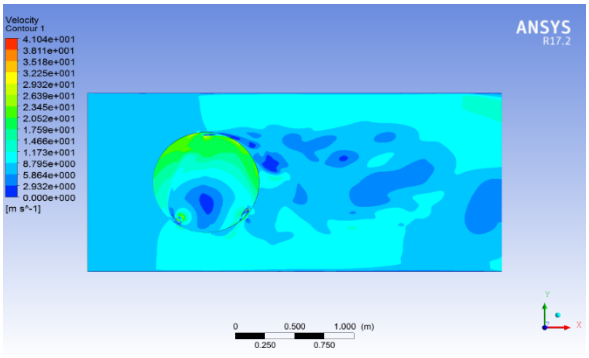

Fig. 5. Velocity distribution through vertical axis wind turbine.

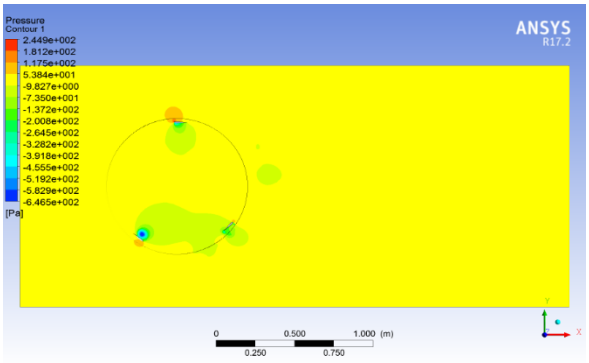

Fig. 6. Pressure distribution through vertical axis wind turbine.

Figures 7 and 8 show velocity zones. As stated earlier, that the velocity would increase at throat section indicated and its magnitude was shown by the scale.

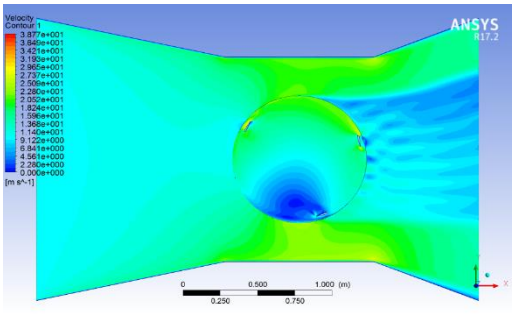

Fig. 7. Convergent-divergent duct velocity distribution inlet angle 12° and outlet angle 20°.

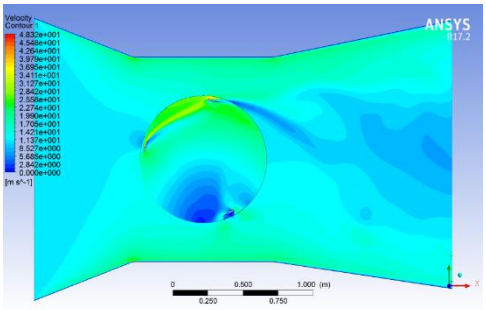

Fig. 8. Convergent- divergent duct velocity distribution inlet angle 20° and outlet angle 12°.

It was noted that the average velocity was raised to more than 20 m/s at inlet angle 12°, while the maximum velocity attained is more than 22 m/s at inlet angle 20°. Similarly, in pressure profile, it decreases in throat area shown in Figs. 9 and 10. In both the cases, a low-pressure region was created in the throat, which is responsible to draw more air. The pressure difference in each region of venture is due to the variation in cross sectional areas. The wind speed increases depending on the difference in cross sections and based on the Bernoulli and venture principles.

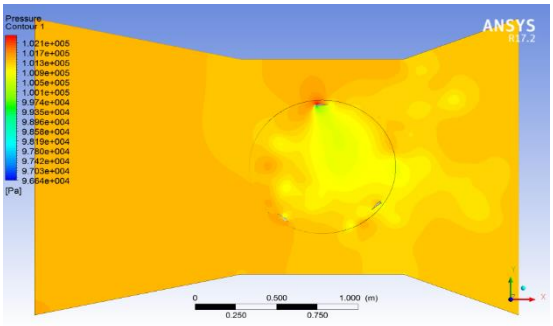

Fig. 9. Convergent divergent duct pressure distribution inlet angle 12° and outlet angle 20°.

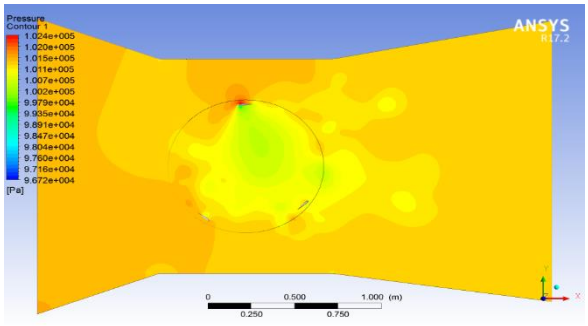

Fig. 10. Convergent divergent duct pressure distribution inlet angle 20° and out let 12°.

Results in Fig. 11 shows that the larger the open angle of the duct lead power coefficient cap is higher. This Cp at TSR equal 1.5 for the convergent-divergent duct increased by 39.024% when the opening angle 20° and exit angle 12°, and the power coefficient enhanced by 35.89% for opening angle of convergent – divergent 12° and exit angle equal 20°. Figure 12 shows the power coefficient against TSR calculated by ANSYS. For two cases of convergent-divergent duct system configuration simulation, power coefficient is obtained and it is compared with analytical solution as shown in Figs. 13 and 14. Reasonable agreements were observed in all cases of the simulation.

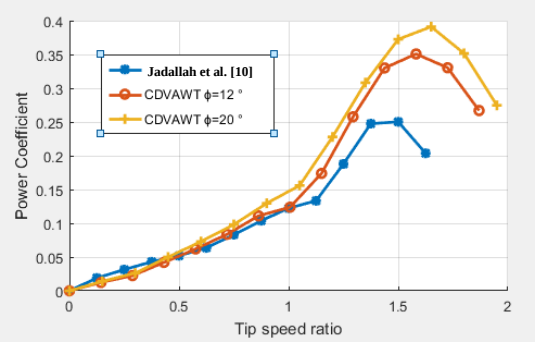

Fig. 11. Power coefficient for convergent ducted wind turbine with TSR.

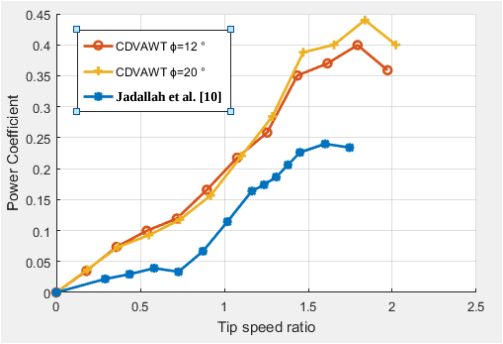

Fig. 12. Power coefficient for ducted wind turbine with TSR.

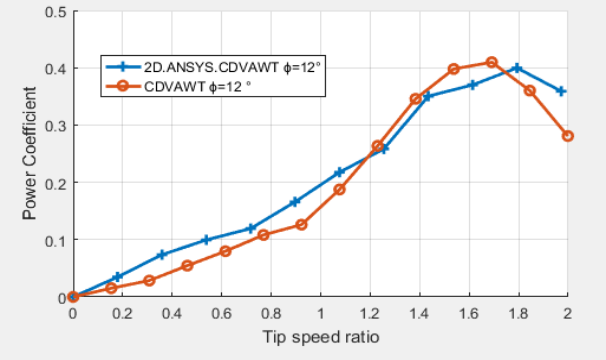

Fig. 13. Coefficient of performance for ducted wind turbine with inlet angle 12°.

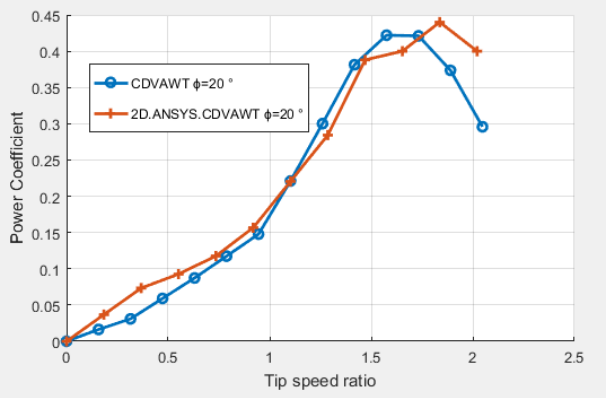

Fig. 14. Variation of CP for ducted wind turbine with TSR for inlet angle 20°.

5. Conclusions

Numerical and analytical predictions of the performance of the ducted vertical axis wind turbine (Darrius -three blades) were achieved in this work employing an adaptable convergent-divergent duct to enhance the performance of the duct VAWT by 35.89% and 39.024% for inlet angle 12° and 20° respectively. This is due to the accessibility to impart more flow rate. This technology may be considered as a promising mechanism, especially when it will be used in urban and low wind speed regimes utilizing the gates and structures providing such passages.

Nomenclatures

A	Area, m^2
Cp	Power coefficients
D_1	Inlet diameter of duct, m
D_2	Outlet diameter of duct, m
k	Turbulent kinetic energy, m^2/s^2
L	Duct length, m
P	Pressure, Pa
t	time, s
V_∞	Free stream velocity, m/s

Greek Symbols

ε	Area ratio
η_c	Convergent duct efficiency
η_d	Divergent duct efficiency
μ	Dynamic viscosity, N s/m^2
μ_{pf}	Back pressure coefficient
ρ	Air Density, kg/m^3
ϕ	Duct Angle, degree
ω	Angular velocity, rad/s

Abbreviations

TSR	Tip Speed Ratio
CDVAWT	Convergent-Divergent Vertical Axis Wind Turbine
VAWT	Vertical Axis Wind Turbine

References

1. Kannan, T.S.; Mutasher, S.A.; and Kenny Lau, Y.H. (2013). Design and flow velocity simulation of diffuser augmented wind turbine using CFD. *Journal of Engineering Science and Technology* (*JESTEC*), 8(4), 372-384.
2. Shires, A.; and Kourkoulis, V. (2013). Application of circulation controlled blades for vertical axis wind turbines. *Energies*, 6(8), 3744-3763.
3. Alaimo, A.; Esposito, A.; Messineo, A.; Orlando, C.; and Tumino, D. (2015). 3D CFD analysis of a vertical axis wind turbine. *Energies*, 8(4), 3013-3033.
4. Lanzafame, R.; Mauro, s.; and Messina, M. (2014). 2D CFD modeling of H-Darrieus wind turbines using a transition turbulence model. *Energy Procedia*, 45, 131-140.
5. Fujisawa, N.; and Shibuya, S. (2001). Observations of dynamic stall on Darrieus wind turbine blades. *Journal of Wind Engineering and Industrial Aerodynamics*, 89(2), 201-214.

6. Kim, D.; and Gharib, M. (2013). Efficiency improvement of straight-bladed vertical-axis wind turbines with an upstream deflector. *Journal of Wind Engineering and Industrial Aerodynamics*, 115, 48-52.
7. Chaudhari, C.D.; Waghmare, S.A.; and Kotwal, A.P. (2013). Numerical analysis of venturi ducted horizontal axis wind turbine for efficient power generation. *International Journal of Mechanical Engineering and Computer Applications*, 1(6), 090-093.
8. Ohya, Y.; Karasudani, T.; Sakurai, A.; Abe, K.-I.; and Inoue, M. (2008). Development of a shrouded wind turbine with a flanged diffuser. *Wind Engineering and Industrial Aerodynamics*, 96(5), 524-539.
9. Kumar, N.M.; Subathra, M.S.P.; Cota, O.D. (2015). Design and wind tunnel testing of funnel based wind energy harvesting system. *Procedia Technology*, 21, 33-40
10. Jadallah, A.A.; Mahmoud, D.Y.; and Farhan, H.A. (2016). Performance evaluation of the vertical axis wind turbine with various rotor geometries. *Al-Qadisiyah Journal of Engineering Sciences*, 9(4), 571-584.
11. Khamlaj, T.A.; and Rumpfkeil, M.P. (2017). Theoretical analysis of shrouded horizontal axis wind turbines. *Energies*, 10(1), 38.
12. Abu-El-Yazied, T.G.; Ali, A.M.; and Montasser, O.A. (2014). Optimization of Wind duct geometry for maximizing power generation of ducted vertical turbines. *IOSR Journal of Engineering* (*IOSR-JEN*), 4(10), 11-19.
13. Wang, F.; Bai, L.; Fletcher, J.; Whiteford, J.; and Cullen, D. (2008). The methodology for aerodynamic study on a small domestic wind turbine with scoop *Journal of Wind Engineering and Industrial Aerodynamics*, 96(1), 1-24.
14. Dannecker, R.K.W.; and Grant, A.D. (2002). Investigations of a building integrated ducted wind turbine module. *Wind Energy*, 5(1), 53-71.
15. Oosthuizen, P.H.; and Carscallen, W.E. (2013). *Introduction to compressible fluid flow*. (2nd Ed.), CRC Press.
16. van Dorst, F.A. (2011). *An improved rotor design for a diffuser augmented wind turbine; improvement of the DonQi urban Windmill*. M.Sc. Thesis. Department of Mechanical Engineering, Eindhoven University of Technology.
17. Menter, F.R. (1994). Two-equation eddy-viscosity turbulence models for engineering applications. *AIAA Journal*, 32(8), 1598-1605.